Deep Learning Pixel Classification Methods and Remote Sensing of Avalanches in Synthetic Aperture Radar Imagery

by

David Harris

A Capstone submitted to Johns Hopkins University in conformity with the requirements for

the degree of Master of Geographic Information Systems

Baltimore, Maryland

May, 2021

Abstract

GIS methods have come to assist avalanche forecasters in understanding avalanche volatility in regions across the globe. Yet, despite recent advances, there has yet to be discovered a method using existing imagery data to determine a complete avalanche history of a forecasting area over a given season that is highly accurate. This capstone project builds on prior research to offer an exploratory methodological approach to consider avalanches pixel classification with a characteristic signature that may be detected using U-Net and deep learning tools. The proposed pixel signature is derived from an exaggerated change detection RGB composite raster based on a before and after Synthetic Aperture Radar (SAR) granule in an orbit to detect the specific avalanche signature in an area. These images are fed into a deep learning model that was developed and consumed in ArcGIS Pro, and may be used to identify avalanche paths in a similar RGB composite image. The effectiveness of the results remain inconclusive and are subject to review from an expert in the field.

Primary Reader and Advisor: Prof. Andrew Chapkowski

Secondary Reader: Dr. Heather Hicks

Contents

Abstract..... ii

List of Figures..... iv

1 Introduction: Predictive Avalanche Forecasting and GIS.....1

1.1. Predictive Avalanche Forecasting and GIS.....1

1.2. Research Purpose.....2

2 Prior Research of Automated Avalanche detection using GIS.....3

2.1. Predictive GIS Methods for Avalanche Forecasting.....3

2.2. Sentinel-1 SAR Based Avalanche Detection.....4

3 Study Area.....5

4 Methods.....6

4.1. Data Preparation of Sentinel-1 IW GRD.....6

4.2. Data Preparation of Tromso Detections Shapefile.....7

4.3. Development of Change Detection Images 9

4.4. Manual digitization of Avalanche Masks.....11

5 Results.....15

6 Conclusions.....17

6.1 Summary.....17

6.2 Limitations and Suggestions for Future Research.....18

7 Works Cited.....19

List of Figures

Figure 1: Study Areas and Satellite Orbit Geometries Near Tromso……..6

Figure 2: Radiometric Terrain Corrected SAR granule and Raw SAR Granule.…….…..…….. 8

Figure 3: Positive Detection Example using VV Polarity……..……10

Figure 4: Positive Detection example using Exaggerated Change Composite Raster……11

Figure 5: Change Detection Image Prone to False Detections……12

Figure 6: Detections from 4/11/2017 in orbit 95……13

Figure 7: Workflow Diagram of Data to Model Pipeline……14

Figure 8: 4/7/2017 Orbit 131 Model Detections……16

Figure 9: 1/15/2019 Orbit 131 Model Detections……17

1. Introduction

1.1 Predictive Avalanche Forecasting and GIS

Snow avalanches are a most common natural disaster in winter alpine environments. They may be triggered with or without human activity, and they have historically been the cause of dozens of avoidable human deaths every year in the United States, and hundreds every year globally (Choubin, et al., 2019, Shweizer, 2008). Where and when avalanches occur is highly dependent on both localized weather events and the spatial landscape, and predicting avalanche volatility has traditionally relied on in-the-field snow assessments in avalanche prone areas to extrapolate generalized danger (Schweizer et al., 2008). In recent years, avalanche forecasting has been supplemented by Geographic Information Systems (GIS) to better understand and catalog the relationship between avalanche paths and the spatial characteristics of their environments. For example, The Swiss Institute for Snow and Avalanche research use GIS to map incoming snowfall and windspeed across their forecasting area to better understand potential slide areas as storms come in, and several areas use GIS to produce daily maps of known avalanche slides and recent conditions (Mccollister and Birkeland, 2006).

GIS provides the spatial analytical processes and deliverables to determine the patterns that can be used in the decision making, and enables novel insights into the spatial relationships of our world by utilizing powerful computational algorithms and calculations, made available through user-friendly graphical user interfaces (GUI) or robust coding libraries. GIS methods are suited to supplement avalanche forecasting due to the relative ease with which GIS offers a platform to reinforce existing knowledge of avalanche danger and explore different predictive methods based on spatial characteristics. For example, a digital elevation model (DEM) for an area of interest can yield the slope, aspect, or an index for surface roughness at a high resolution to assist in identifying risky areas

avalanche zones. Additionally, land cover data may be used to create masks of avalanche areas that are only prone to occurring in areas with specific land class types to eliminate areas with high tree cover, or highly developed areas among other types with low avalanche probability.

1.2 Research Purpose

The goal of this project is to explore GIS methods that may contribute to avalanche forecasting by building on current methods to locate past avalanche events in satellite imagery, specifically by using synthetic aperture radar (SAR), to contribute to future development of automated methods to identify avalanches based on publicly available data that is not dependent on cloud cover. This study uses the product of prior research to detect avalanches automatically in Sentinel-1 data (Eckerstorfer et al., 2019) to develop avalanche masks to build on prior research using convolutional neural networks to detect avalanches in novel raster combinations (Bianchi et al., 2020). By combining methodological approaches used by Bianchi et al., (2020) and the change-detection images used by Eckerstorfer et al., (2017), this study assesses how a new RGB composite "exaggerated" change-detection image may be used as an input into deep learning neural networks to detect avalanches. The final product of this study is a U-Net pixel classifier that may be deployed within widely used commercial ArcGIS software to locate past avalanches in Sentinel-1 SAR granules. U-Net, a deep learning neural-network, was originally developed to solved complex semantic segmentation in biomedical images (Ronneberger et al., 2015). It has become a deep learning neural network with many applications to diverse GIS problems over the past years, including identifying damaged infrastructure, identifying building footprints, and land cover classification (Asada et al., 2020, Data et al., 2019). This study attempts to add to the growing body of work applying U-Net to solve geospatial problems.

2. Prior Research of Automated Avalanche Detection Using GIS

2.1 Predictive GIS Methods for Avalanche Forecasting

Scientific approaches to avalanche forecasting have varied from region to region, however there is a well-established consensus on the basic conditions required for snow avalanches to occur in an environment. Avalanches occur on sloped faces between 25 and 55 degrees in most cases and can be broken down into three distinct features in a starting zone, a track, and a runout zone (Blahut et al., 2016, Choubin et al., 2019). Avalanche paths have been modeled and predicted using several different machine learning approaches, and support vector models, and multivariate discriminant analysis have been shown to be effective predictors of avalanche paths (Choubin et al., 2019). These methods use inputs such as slope, proximity to water sources, aspect, terrain roughness, and many other factors to determine avalanche susceptibility of given locations. Random forest, Naïve Bayes, and additive model machine-learning approaches have also been implemented in determining the most critical independent variables associated with avalanche paths (Rahmati et al., 2019).

There have been numerous GIS approaches to identify avalanche paths in remotely sensed data sources. Eckerstorfer et al. (2015) outline the data types of remotely sensed landscape data available for avalanche detection into their three categories: optical imagery, lidar, and ladar. High resolution optical imagery is a proven effective data source in which to locate avalanches, though it can be challenging to collect. Lato et al., (2012) used aerial images to develop an automated object detection method that could identify avalanche paths based on the image signature of the disturbed snow next to undisturbed snow that was 97% accurate. While avalanches detection can be highly effective using aerial imagery, such data can be expensive to acquire and imagery resources are dependent on low-cloud conditions, making them a less reliable resource to detect avalanches (Eckerstorfer et al., 2015). Lidar resources have been used to detect avalanches by measuring the snow depth in an area and

inferring avalanche paths from the difference in mass from the surrounding area from an avalanche path and an avalanche landing area (Prokop, 2008). Similar to optical imagery sources, lidar can be expensive and is reliant on low cloud cover, but as lidar resources become more readily available to the public, more research on possible detections methods using lidar may yield high accuracy results. Finally, space-born SAR data has been used to identify avalanche debris by analyzing the backscatter signature of avalanche landing zones with the surrounding snow signature.

2.2 Sentinel-1 SAR-Based Avalanche Detection

Avalanches were first detected in SAR data in 2001 by comparing two backscatter granules from identical orbits and compiling the images into a composite RGB image (Weismann et al., 2001). Eckerstorfer et al., (2015) first showed that these same methods could be applied to Sentinel-1 SAR images, and Eckerstorfer et al., (2017) used this method to attempt to manually identify a full record of avalanche activity in a small forecasting area in Norway using change detection RGB composites. Eckerstorfer et al., (2019) built on the idea of using the difference between succeeding Sentinel-1 images to detect avalanches to develop a threshold-based method to identify pixel clusters with the greatest difference in value from their pixel neighborhood using VV and VH polarities. The automated process identified 72% of avalanches in a forecasting region in Northern Norway as compared with the manual detection method used by Eckerstorfer et al., (2015) and had as many as 50% of the identified avalanches confirmed to be false detections (Eckerstorfer et al., 2019). Bianchi et al., (2020) deployed a fully convolutional network (FCN) using SAR data from the same region in Norway for the period between October 2014 and October 2017. Their training data was developed by a human expert using the same change detection images used in the first study reviewed above to confirm the validity of the results. They trained the manually detected masks on image stacks composed using difference images between succeeding VV and VH polarities, a combined raster using both difference images squared,

slope, and a topographical feature called potential angle of reach that they developed as part of their approach (Bianchi et al., 2020). Their results showed cases where the neural network was able to detect avalanches missed by the human expert, though overall their accuracy rate was still not as reliable as manual detection.

3. Study Area

This study focuses on a small subset of the same study area as Eckerstorfer et al., (2019) northern province of Troms, Norway. The town and the area surrounding it experience a snowy weather period for 7.5 months of the year, from early October until mid-May (WeatherSpark, 2021). The mountains around Tromso are known as the Lyngen Alps, and they have been the site of numerous studies attempting to locate avalanche paths in SAR imagery. This region is an ideal location to identify avalanche paths in Sentinel-1 SAR datasets because of the mountainous terrain and consistent snowfall and due to its location high in the northern hemisphere. Sentinel-1 collects data along polar orbitals and areas with higher latitude coincide with a higher number of orbit paths than areas closer to the equator. Because Troms is located at a high latitude, there are multiple Sentinel-1 orbit paths that contain ground cover data for the study area. Eckerstorfer et al., (2019) shared a shapefile of automated detections from the entire forecasting region over a four-year period, hereafter referred to as the potential detections shapefile. Within this larger area, this study focuses on a 178 square mile area to the southwest of the town of Lynseidet because it is encompassed in its entirety by three different orbit paths and does not have any large human-made developments. The selected area is shown in red in figure 3 and the larger forecasting area from which the prior detections were discovered is shown in yellow.

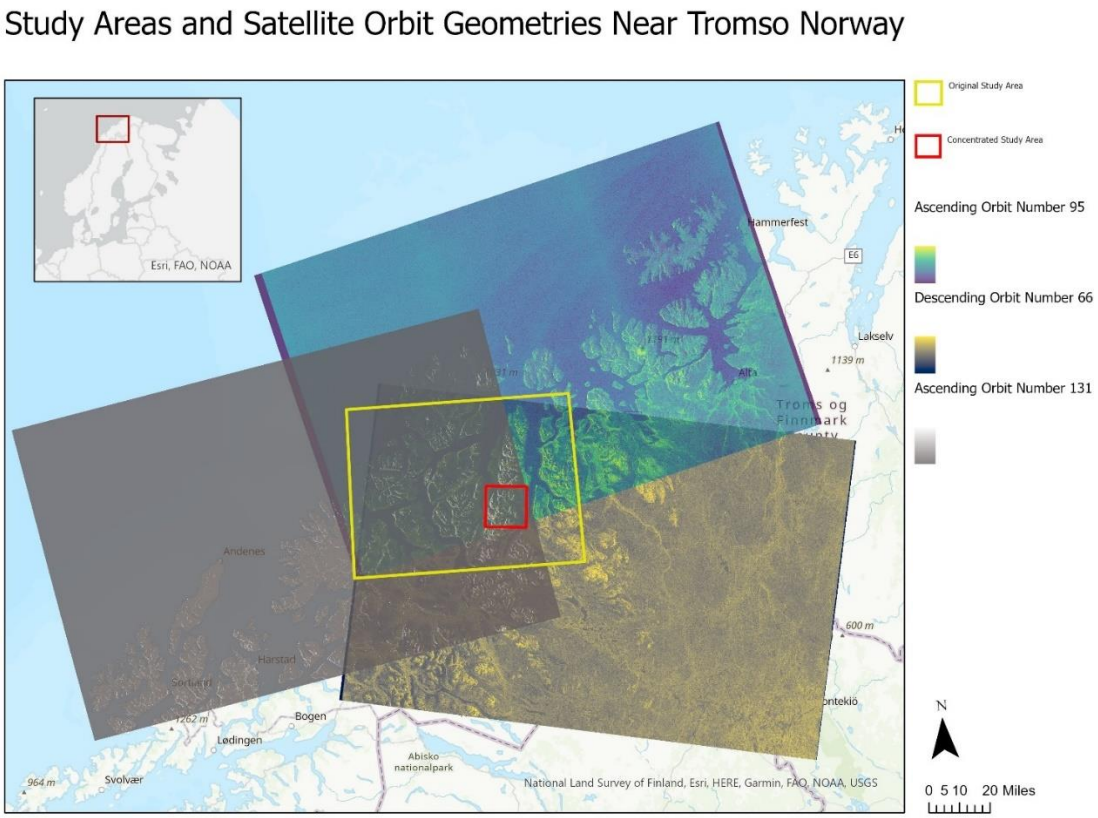

Figure 1: The study area is shown in red and the study area from previous research in yellow, against the three different satellite orbit geometries for which SAR data was acquired.

In the concentrated study area, the avalanche detections from three paths were used to develop training data for automated avalanche detection in the SAR granules.

4. Methods

4.1 Data Preparation of Sentinel-1 IW GRD

The ESA's Sentinel-1 mission captures SAR granules for virtually any given area on Earth every 6 days starting in 2017, or every 12 days for the period prior to the release of Sentinel-1B. Sentinel-1 products are available in two different formats: Ground-Range Detected (GRD), and Single Look Complex (SLC). GRD products are a fraction of the size and have a slightly reduced spatial resolution than SLC products and are available pre-processed such that the slant-range coordinates are projected onto the earth's surface in WGS1984 (Eckerstorfer et al., 2017). GRD products also contain two

polarities for each granule: Vertical, Vertical polarity, (VV) and Vertical, Horizontal polarity (VH). SLC products are required for analysis using interferometry, however GRD products are preferred to perform change detection for avalanches in mountainous environments due to their lower storage requirements and preprocessed characteristics. While the ESA process data such that it is already projected, the GRD images must be ground-truthed to the terrain in an area of interest. The algorithm to terrain-correct a granule is dependent on orbit metadata for the SAR image and satellite path, as well as a high-quality DEM to ground truth the image. This process creates distortions in a result in the form of layover and shadow regions, which represent the areas

To acquire Sentinel-1 GRD SAR data, granules were retrieved using the Google Earth Engine (GEE) Python API. The decision to acquire the Sentinel-1 data from GEE versus the Copernicus Open Data Hub, which is another popular open data source for complete Sentinel-1 SAR data and includes more complete metadata, was made due to the relative ease with which radiometric terrain corrections (RTC) may be made using GEE. RTC is the process of making sure the pixels derived from the side-angle Sentinel-1 radar are displayed over the terrain they capture. Figure 2 shows an example of a RTC image and a raw Sentinel-1 granule. This project used previously developed python scripts to execute the RTC within the GEE API on the Google Earth Engine servers and return clipped raster products to a private google drive from where the data could be downloaded to disk and manipulated further. The DEM used to execute the terrain corrections was a high quality 10-meter resolution DEM dataset provided by prior researchers and loaded into the GEE environment using the GEE browser-based user interface. Using GEE in this way was more efficient to store, download, and process the SAR datasets than acquiring the raw granules in full from Copernicus open data hub and storing them on disk. VV and VH sigma-nought backscatter raster datasets as well as layover and shadow datasets were downloaded for orbits 66, 95, and 131 and clipped to the study area for every date that a given orbit

was collected by the Sentinel-1 sensors between January 1 and May 1 for the winter seasons of 2016, 2017, and 2019. In total, 205 image dates were collected, retrieving 4 different raster datasets for each date. Once the data was downloaded to disk, each product was transformed from a geotiff raster product into a file geodatabase raster dataset and projected into the UTM Zone 33 North coordinate reference system.

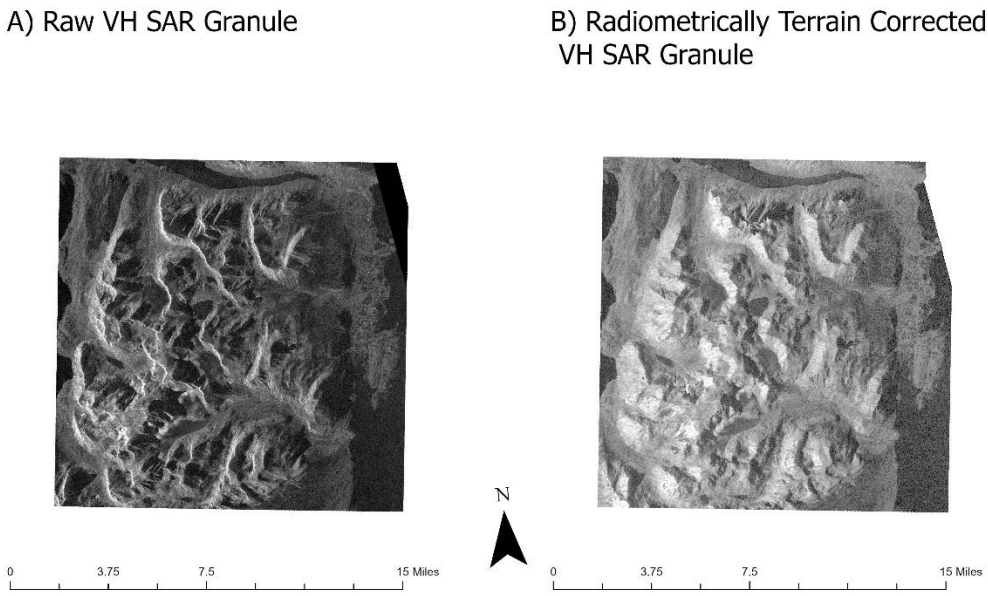

Figure 2: A raw VH Sentinel-1 IW GRD SAR granule for the area of interest downloaded directly from Copernicus Open Access Hub and a radiometrically terrain corrected VH granule acquired from Google Earth Engine from the same source Sentinel-1 dataset

4.2 Data Preparation of Tromso Detections Shapefile

The potential detection shapefile from Eckerstorfer et al., (2019) identified avalanches with a positive success rate of around 72% and with a false positive rate that was around 52% (Eckerstorfer, 2019). The shapefile contained 59,336 detections in total over a study area that was roughly 150 by 100 kilometers. To limit the number of detections to an appropriate amount of data for this project, only 3 seasons were considered and only 3 of the 10 satellite geometries were selected that completely contain the study area. The time periods from which detections were collected and Sentinel-1 data was acquired were from December 1- May 1 for 2016,2017, and 2019. For the three satellite orbits in

the study area for the specific time-slices discussed, the potential detection shapefile identified 272 avalanche shapes in 2016, 1,426 in 2017, and 1,461 in 2019. Detected avalanche pixels from this shapefile were filtered out by date and orbit path, exported into corresponding geodatabases for each date, and projected into UTM Zone 33 North.

4.3 Development of Change Detection Images

The detected features from the Tromso detections shapefile within the time frame and geographic boundaries of the study were clipped to exclude certain land cover classes in the region according to practices described by Eckerstorfer et al., (2019) such that detections occurring within a large glacier in the study area were excluded from consideration. The remaining potential detections were evaluated based on their appearance in the Sentinel-1 SAR change detection images that were first developed in 2001 (Weissman et al., 2001). A change detection image is an RGB composite raster based on a single polarity of a SAR granule. These images are developed using a VV raster in the R and B channels of a composite raster, and by showing the VV granule of the succeeding SAR product in the G channel. An example of a positive detection that was positively reflected in the shapefile as expressed in a change detection image is shown in figure 3. A change detection image was constructed for every date a SAR dataset was acquired for each of the three paths except for the very first dataset in an orbit (for these datasets, no reference image was acquired) and were used to assist in the process of manually digitizing the training shapes for the project.

The novel aspect of this studies methodological approach is the development of an exaggerated change detection image. These exaggerated images draw on the raster calculations of Bianchi et al., (2020) to use a difference of each individual polarity in the R and B channels, and in the G channel is a combined exponential difference band. The difference of each polarity may be expressed as the

succeeding image from and identical orbit minus the preceding image. In the difference image, area with greater differences are highlights and the rest of the image is more uniform. The band set in the G channel of the composite raster is developed by rescaling the difference between each individual band using a mean multiplier and standard deviation multiplier transformation, squaring each

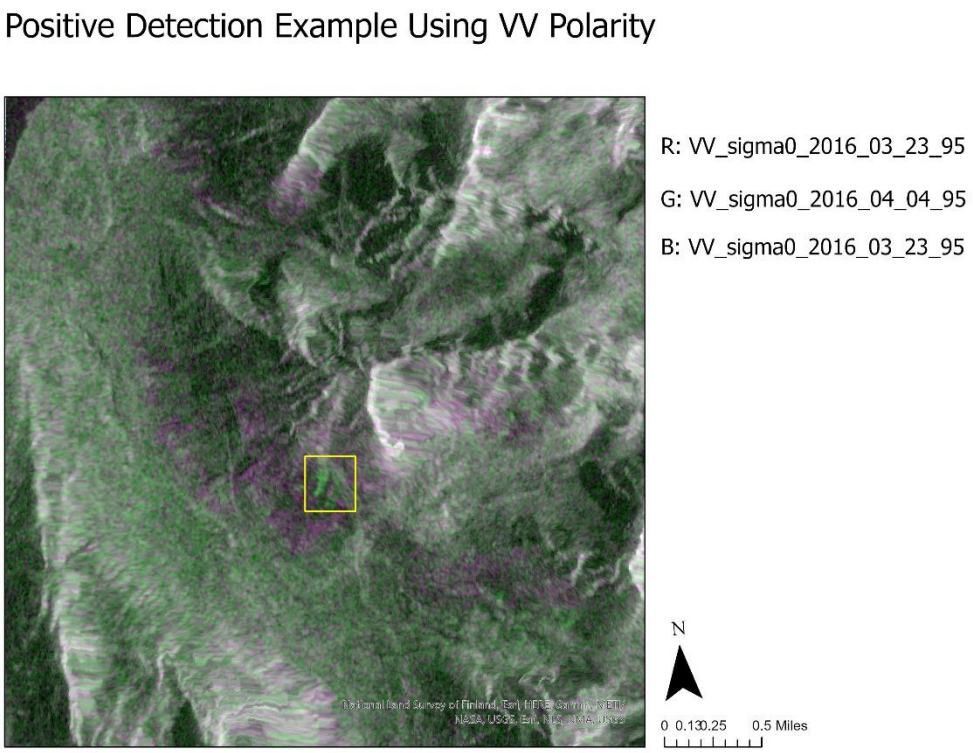

Figure 3: An original change detection image from 4/4/2016 from Sentinel-1 orbit path number 95. In the R channel of the composite raster is the VV sigma-nought backscatter signature from orbit 95 acquired on 3/23/2016. This same image is also shown the in B channel of the composite. The VV sigma-nought backscatter signature from orbit 95 collected on 4/4/2016 is shown in the G channel of the composite. In the yellow square, a classic example of a positive detection is displayed.

rescaled image, and then multiplying the two squared images. The result is an abstract RGB composite image in which avalanche paths appear as bright violet shapes with defined edges in front of a greener background as shown in figure 4. The exaggerated heightened edges and difference signatures in all three channels are theorized to enable detection in a U-Net pixel classification model, and are used as the input data used by this study.

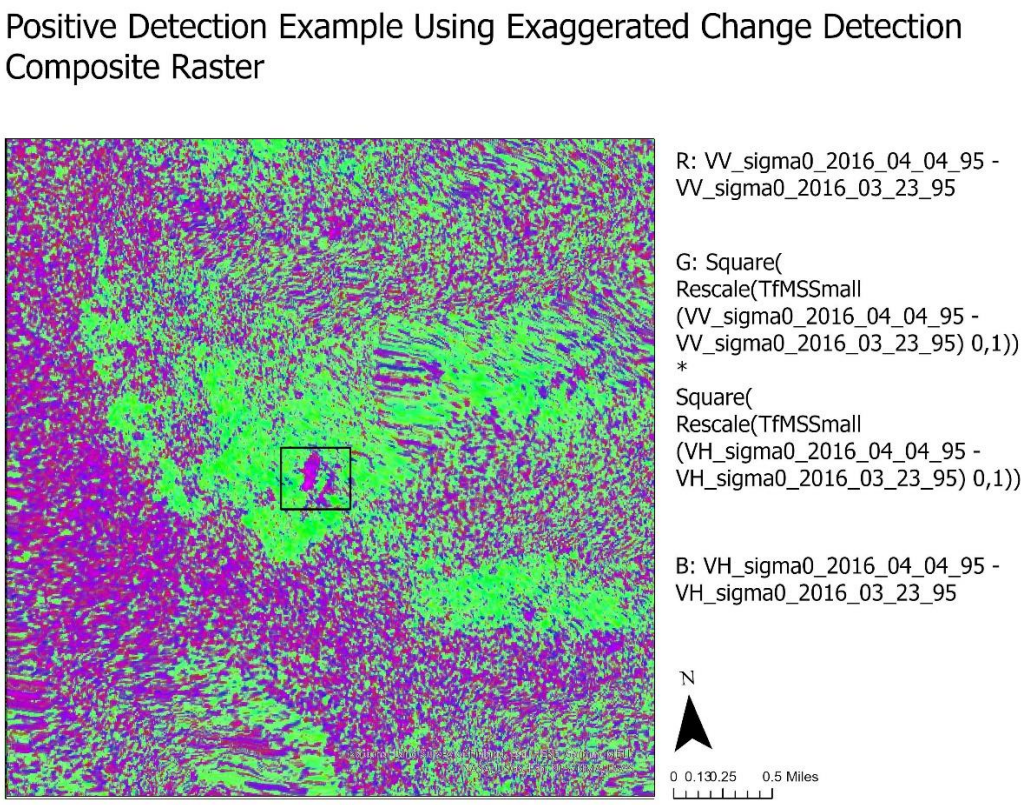

Figure 4: Exaggerated difference composite where avalanche paths show up as a bright violet streak against a green background. The R channel input is the VV sigma nought backscatter acquisition from orbit 95 in which a detection is theorized to be visible acquired on 4/4/2016 minus the preceding VV sigma-nought backscatter acquisition from orbit 95 on 3/23/2016. In the B channel is the corresponding VH sigma-nought backscatter acquisition. In the G channel is the product of each of these images rescaled using the TfMSSmall function and squared.

4.4 Manual Digitization

Using the potential detection shapefile, avalanche path masks were evaluated by examining the results in the original change detection image and digitizing a polygon shape over the corresponding pixels in the exaggerated change detection image. The process of identifying which potential detections to include and which detections to disregard was judged based on the overall quality of the original change detection image, as well as the shape and position of the detection itself. For example, detections that appeared to correlate with specific topographic features and the shapes of such paths were not consistent with the expected avalanche runout shape as articulated in prior research were not digitized. Figure 5 shows a change detection image with several detections that

were not considered valid.

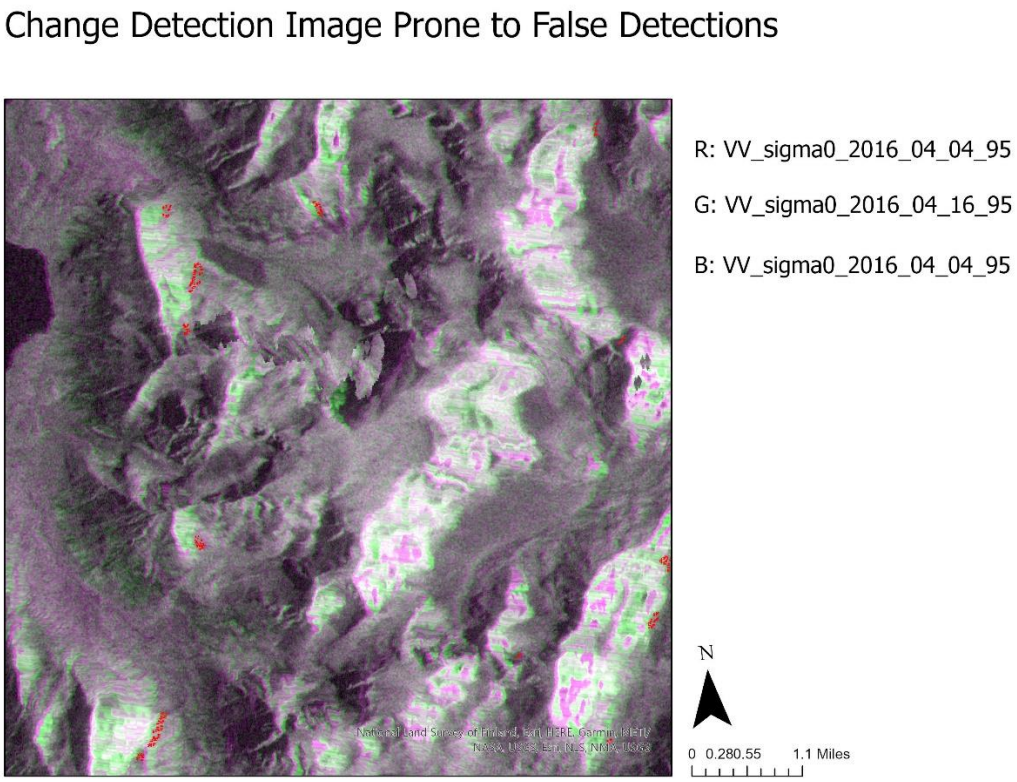

Figure 5: A change detection image with false detections shown as a dashed red line. In this image, The VV backscatter difference is consistently heightened in layover areas, and seem to correlate with topographic features. One possible theory for such differences is fresh snow between the two acquisition dates. This could lead to a very slight change in most areas that appears heightened in layover zones as that change gets stretched out. Detections from this date appear as layover zones transition back into the rest of the image.

On such dates, all the potential detections from prior research were discarded. In cases where a detection showed the characteristic shape and color in the original change detection images, new shapes were created that matched the corresponding pixels in the exaggerated image, which were not typically in the exact same place as the original potential detections. This process was accomplished within the ArcGIS Pro editing environment. Figure 6 shows an example of a positive detection assumed to be correct due to the shape and location of the potential detection in the original change detection images. Where to delineate the masks from the surrounding pixels will determine which pixels the deep learning model will assume are avalanche debris.

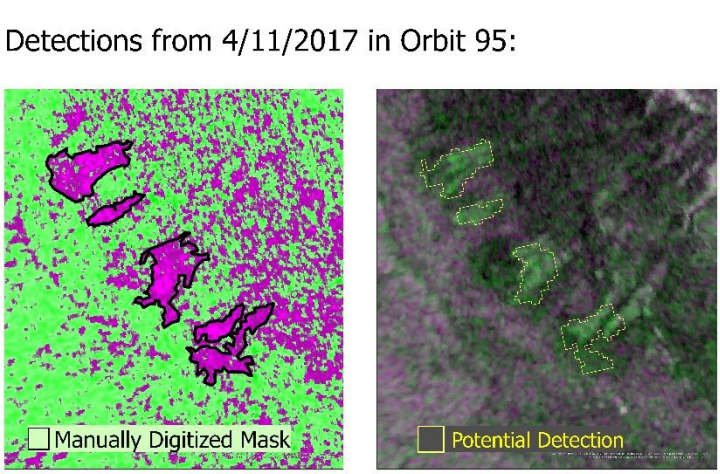

Figure 6: The manual result displayed over an exaggerated change detection image next to the original potential detection over the original change detection image from 4/11/2017 in orbit 95. The image on the left shows the masks that were used to train the U-Net model.

This process is subject to refinement, and the approach in this study was to create masks around the sharpest clearest lines in the detection area. In total, after discarding many potential detections, 207 avalanche path masks were created in 22 different change detection images. In each of the polygon feature classes a class value field named 'classvalue' was added and calculated to be 1. This is to indicate to the deep learning process that all the shapes belong to the same class indicating that the shape represents an avalanche runout path. Each change detection raster was then exported to an 8-bit unsigned tiff raster dataset on disk according to Esri's recommendation when using deep learning tools with RGB raster data. Using the built-in 'Export Training Data for Deep Learning' tool, each of the polygon feature classes and 8-bit training rasters to generate 128 x 128 pixel chips and labeled masks. A 64 -bit stride value was selected to that the training data could evaluate detections from partial images. Using the arcgis.learn python module, a U-Net classifier was trained against the exported data in batches of 4 for 100 epochs. The resulting model was then saved and could be used as an input into the 'Classify Pixels Using Deep Learning' tool in ArcGIS Pro. Figure 7 shows a workflow diagram that outlines the steps described above to preprocess Sentinel-1 SAR granules to create a U-Net avalanche classifier. The different python environments are included to indicate that there are incompatibilities between the GEE API and the ArcGIS default python environment. A separate virtual environment is required to reproduce that portion of this project. Additionally, to use the deep

learning tools in ArcGIS pro, a separate cloned environment is required, and Esri documents detailed

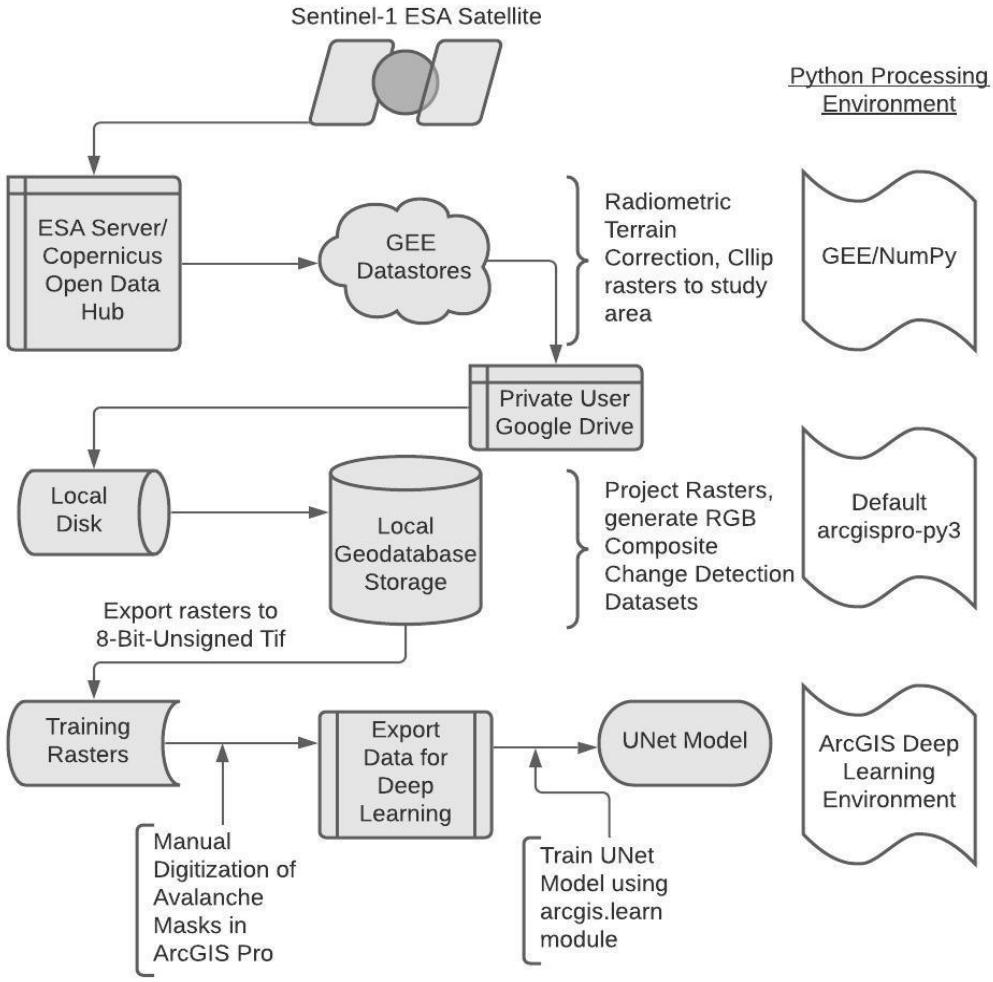

Figure 7: Workflow diagram showing data storage and processing from ESA sentinel-1 satellite to output of a trained U-Net model that may be used in ArcGIS pro to detect avalanche paths in the change detection images generated using raster functions. The different python environments required for each step of processing is described.

instructions on how to recreate the required environment for these tools (Esri, 2021). To run the trained U-Net classifier, test datasets were clipped to exclude detections on glacier land-types, and a mask was created to only assess data on with a slope between 5 and 55 degrees. This would admittedly miss runout zones that are possible on flat terrain beneath very large avalanches, but this mask would serve to eliminate additional false detections above possible runout zones as well as flat, coastal areas that yield inconsistent backscatter signatures. The model was run against two test

images, although one of the two was included in the training set, and would be more likely to show positive results on paths that were originally entered as inputs into the model.

5. Results

The images below show the side-by-side comparison of the resulting avalanche paths from the automated detection process that was used to guide the data development alongside the output from the trained U-Net model. Figure 8 shows some of the detections when the model was run on an image that was originally included in the training dataset, and Figure 9 shows several detections from a test image that was not included in the training set. The detections identified from April, 7 2017 in orbit path 131 had 18 potential detections in the original shapefile, and 27 in the U-Net output after removing detections below 1,000 square meters in area. Visually looking through each output in the result determined 10 of these detections to be positive, 7 to be false detections, and another 10 to be ambiguous, and subject to review from an expert. The original shapefile contained 28 detections from January 15, 2019 in orbit 131, and the U-Net results contained 20 after eliminating detections below 1,000 meters in area. Among these 20 shapes, 11 were determined to be valid detections, 4 were determined to be false, and another 5 were determined to be ambiguous and subject to review from an expert in the field.

The results of this project build upon the prior work of Eckerstorfer et al (2019) and Bianchi et al (2020) to confirm that there is further cause to investigate using deep learning pixel classification methods to detect avalanche paths in Sentinel-1 SAR data. The model produced did not ultimately prove to be better at detecting avalanches than prior methods, but the possible efficacy of this

approach remains inconclusive due to several limitations of this study. The partial overlap in detections displayed in the results given the low sample size of input detections in this study indicates cause for future research into U-Net classification of avalanche paths in Sentinel-1 SAR data.

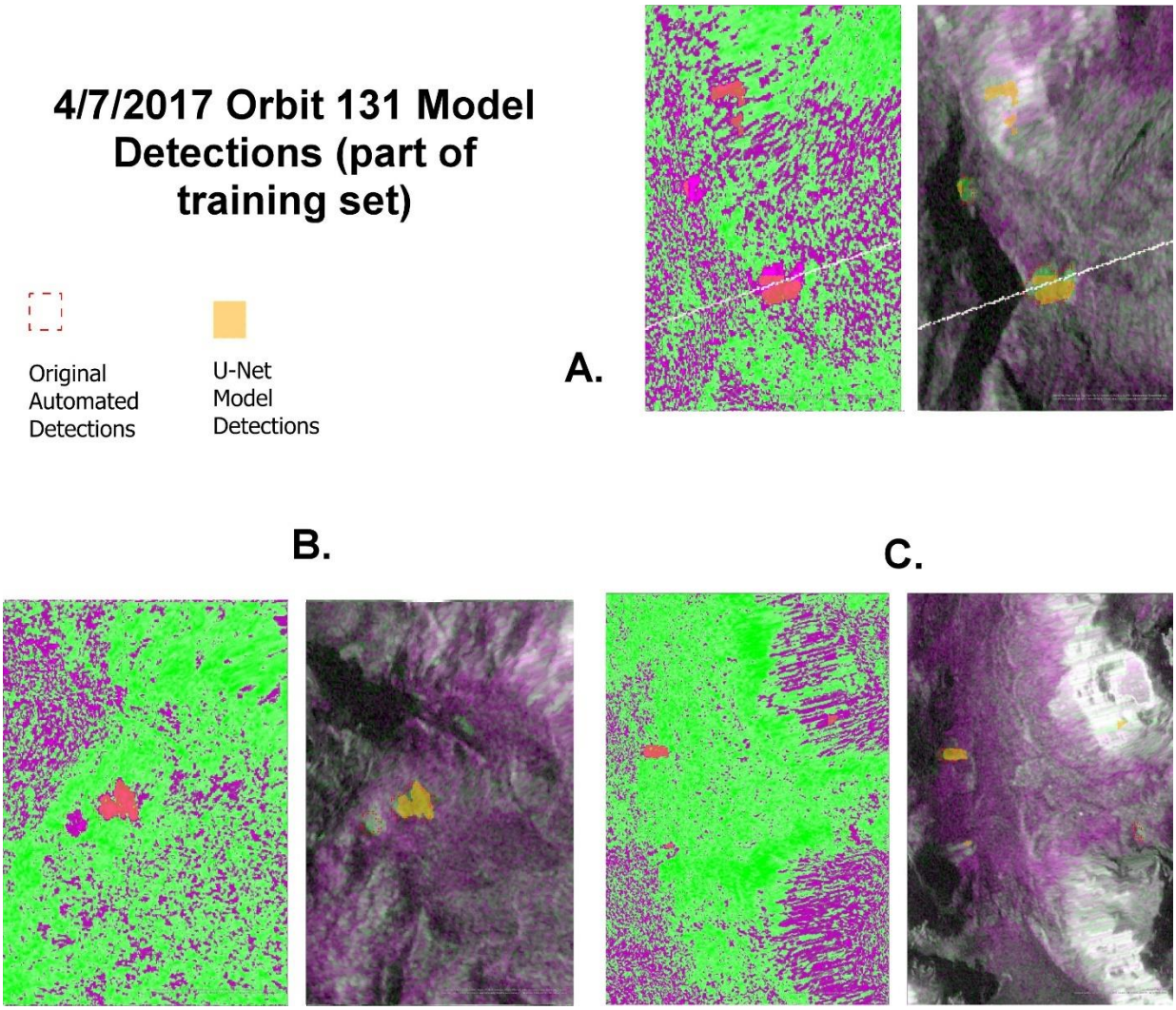

Figure 8: Three examples of positive correlation between the original automated method and the U-Net Classifier, as well as examples of ambiguous differences between the two models. Figure 8.A shows the two original detections confirmed, although one of the two is cut off due to it's location on a land area classified as a glacier. Two additional detections appear to be ambiguous as they occur in a layover area that can yield inconsistent results. Figure 8.B shows one of two original detections confirmed, and both the original method and the U-Net classifier appear to have missed a small avalanche path. Figure 8.C shows one of two original detections confirmed, one false detection, and one positive detection that was not part of the original set.

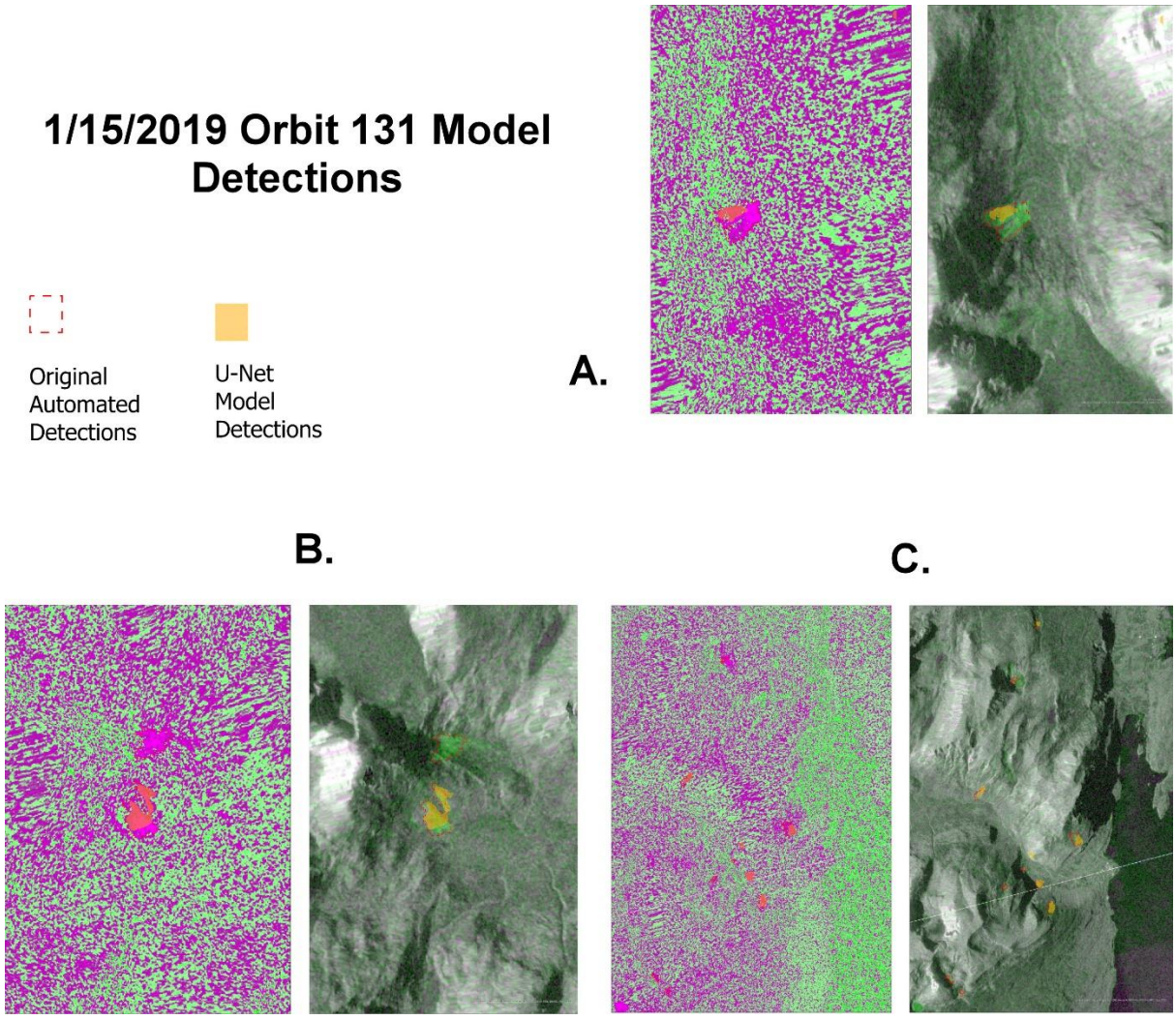

Figure 9: A comparison of three side-by-side detections from 1/15/2019 in orbit 131. 9.A Shows a single large detection confirmed by the U-Net classifier, although it is cut off due to it's location on a land area classified as a glacier. 9.B shows 2 out of 3 original detections confirmed by the U-Net classifier. 9.C shows 6 detections confirmed by both classification methods, 4 detections present in the original shapefile, though 2 appear to be errant, and 1 errant detection from the U-Net classifier.

6. Conclusions

6.1 Summary

This study outlines the process to download and process RTC Sentinel-1 IW GRD SAR data, and documents an attempt to implement a pixel classification neural network using ArcGIS Pro built in deep learning functions to identify avalanche paths in RGB composite images created from two

succeeding Sentinel-1 acquisitions in a single orbit. 207 training shapes were identified in these images based on visual confirmation of possible detections from prior avalanche detection algorithms that were identified over 22 different acquisition dates. The primary contribution of this project to prior research efforts to identify avalanches in SAR imagery is the development of a novel "exaggerated" change-detection RGB composite raster that may be used as the sole training source in the U-Net classifier. The results of how this method performs comparted to other automated methods is inconclusive due to the low sample-size of the verified detections identified by the model.

6.2 Limitations and Suggestions for Future Research

There are several limitations of this study. First, the training samples used in this study were not verified avalanche paths but were inferred drawing from prior research efforts to identify avalanche debris in Sentinel-1 backscatter. More reliable training data where every detection is verified by an expert in a region or in recognizing avalanche paths could improve the quality of the model. Additionally, this model was developed with just over 200 training shapes. Despite the efforts made in the exaggerated change detection images that were developed in this study, identification of avalanche debris remains a subtle classification and a greater magnitude of samples can crucially change the accuracy of the deep learning model. Another suggested modification that may improve the efficacy of the model would be to create more than one avalanche class. Not all avalanches exhibit similar backscatter signatures due to the differences in their possible size, snow type and on their potential cause. A more developed model with a greater number of samples could split the training detections into different classes based on these characteristics to achieve greater accuracy. With only one class of avalanches, as a model is trained on a greater number of small avalanche areas, accuracy of larger avalanches would be expected to be diminished. Additionally, the exaggerated change detection image that was developed in this project is one experimental approach many

possible raster calculations that may be used to combine succeeding Sentinel-1 granules into a single image. For example, using the MSSmall transformation to rescale the difference raster datasets to generate the G channel of the composites used in this study is a step that introduces a dramatically different result than using a linear transformation. Small difference in the composition of the change detection images may yield results of higher or lower accuracy. Additionally, other raster combinations could be added to different channels to enhance the model. For example, multiplying the elevation by the slop or introducing surface terrain roughness could be interesting independent variables to include, hat may yield encouraging results as a single raster combination in a single channel of an RGB composite raster. Tweaking these inputs as well as other model parameters such as the window-size of the training chips would be important steps to consider when attempting to develop a more robust neural network to detect avalanche paths in Sentinel-1 SAR imagery.

7. Works Cited

Asada, T., Kachi, K., & Arimura, M. (2020). *Exhaustive Pavement Inspection on Residential Roads Using Car-Mounted Cameras and U-Net*. 2020–2021.

"Average Weather in Tromsoe," WeatherSpark, last accessed May 5, 2021. https://weatherspark.com/y/84211/Average-Weather-in-Troms%C3%B8-Norway-Year-Round#:~:text=The%20snowy%20period%20of%20the,equivalent%20accumulation%20of%201.7%20inches.

Bianchi, F. M., Grahn, J., Eckerstorfer, M., Malnes, E., & Vickers, H. (2020). *Snow avalanche segmentation in SAR images with Fully Convolutional Neural Networks*. 1–8.

Blahut, J., Klimeš, J., Balek, J., Hájek, P., Červená, L., & Lysák, J. (2017). Snow avalanche hazard of the Krkonoše National Park, Czech Republic. *Journal of Maps*, *13*(2), 86–90. https://doi.org/10.1080/17445647.2016.1262794

Choubin, B., Borji, M., Mosavi, A., Sajedi-Hosseini, F., Singh, V. P., & Shamshirband, S. (2019). Snow avalanche hazard prediction using machine learning methods. *Journal of Hydrology*, *577*(March), 123929. https://doi.org/10.1016/j.jhydrol.2019.123929

Esri, "deep-learning-frameworks," Github Repository. Last accessed May 5 2021. https://github.com/Esri/deep-learning-frameworks

Data, M. G. I. S., Li, W., He, C., Fang, J., Zheng, J., & Fu, H. (2019). *Semantic Segmentation-Based Building Footprint Extraction Using Very High-Resolution Satellite*. https://doi.org/10.3390/rs11040403

Eckerstorfer, M., & Malnes, E. (2015). Manual detection of snow avalanche debris using high-resolution Radarsat-2 SAR images Cold Regions Science and Technology Manual detection of snow avalanche debris using high-resolution Radarsat-2 SAR images. *Cold Regions Science and Technology*, *120*(September), 205–218. https://doi.org/10.1016/j.coldregions.2015.08.016

Eckerstorfer, M., Malnes, E., & Müller, K. (2017). A complete snow avalanche activity record from a Norwegian forecasting region using Sentinel-1 satellite-radar data. *Cold Regions Science and Technology*, *144*(December 2016), 39–51. https://doi.org/10.1016/j.coldregions.2017.08.004

Eckerstorfer, M., Vickers, H., Malnes, E., & Grahn, J. (2019). Near-real time automatic snow avalanche activity monitoring system using sentinel-1 SAR data in Norway. *Remote Sensing*, *11*(23), 1–23. https://doi.org/10.3390/rs11232863

Karbou, F., Coléou, C., Lefort, M., Deschatres, M., Eckert, N., Mart-, R., Charvet, G., & Dufour, A. (2018). *MONITORING AVALANCHE DEBRIS IN THE FRENCH MOUNTAINS USING SAR OBSERVATIONS FROM SENTINEL-1 SATELLITES*. 344–347.

Lato, M. J., Frauenfelder, R., and Bühler, Y (2012). *Automated detection of snow avalanche deposits: segmentation and classification of optical remote sensing imagery*, Nat. Hazards Earth Syst. Sci., 12, 2893–2906, https://doi.org/10.5194/nhess-12-2893-2012, 2012.

Mccollister, B. C., & Birkeland, K. (2006). Using Geographic Information Systems for Avalanche Work. *Avalanche Review*, *24*(4), 10–11.

Prokop, A. (2008). Cold Regions Science and Technology Assessing the applicability of terrestrial laser scanning for spatial snow depth measurements. *Cold Regions Science and Technology*, *54*(3), 155–163. https://doi.org/10.1016/j.coldregions.2008.07.002

Rahmati, O., Ghorbanzadeh, O., Teimurian, T., Mohammadi, F., Tiefenbacher, J. P., Falah, F., Pirasteh, S., Ngo, P. T. T., & Bui, D. T. (2019). Spatial modeling of snow avalanche using machine learning models and geo-environmental factors: Comparison of effectiveness in two mountain regions. *Remote Sensing*, *11*(24). https://doi.org/10.3390/rs11242995

Ronneberger, O., Fischer P., and Brox T. U-net: Convolutional networks for biomedical image segmentation. In MICCAI, pages 234–241. Springer, 2015. 2, 3

Schweizer, J., Kronholm, K., Jamieson, J. B., & Birkeland, K. W. (2008). Review of spatial variability of snowpack properties and its importance for avalanche formation. *Cold Regions Science and Technology*, *51*(2–3), 253–272. https://doi.org/10.1016/j.coldregions.2007.04.009

Vollrath, A., Mullissa, A., & Reiche, J. (2020). Angular-based radiometric slope correction for Sentinel-1 on google earth engine. *Remote Sensing*, *12*(11), 1–14. https://doi.org/10.3390/rs12111867

Wiesmann, A., Wegmüller, U., Honikel, M., Strozzi, T., & Werner, C. L. (2001). *Potential and methodology of satellite based SAR for hazard mapping*. *July*, 3–5.